Pergamon

Int. J. Heat Mass Transfer. Vol. 40, No. 1, pp. 73–88, 1997

0017–9310/97 $15.00 + 0.00

PII: S0017–9310(96)00067–1

Effects of surface roughness on water droplet impact history and heat transfer regimes

JOHN D. BERNARDIN, CLINTON J. STEBBINS and ISSAM MUDAWAR†

Boiling and Two-phase Flow Laboratory, School of Mechanical Engineering, Purdue University, West Lafayette, IN 47907, U.S.A.

(*Received* 18 *December* 1995 *and in final form* 8 *February* 1996)

Abstract—Still and high speed photographic techniques and heat transfer measurements were used to study the impact of water droplets on heated surfaces with different roughness. The study encompassed droplet Weber numbers of 20, 60 and 220 and surface temperatures of 100–280°C, covering droplet stability and heat transfer regimes established previously by the authors for polished surfaces. Three different surface finishes, polished, particle blasted and rough sanded, with respective arithmetic average surface roughness values of 97, 970 and 2960 nm, were applied to the test surfaces. While the temperature corresponding to critical heat flux (CHF) was fairly independent of surface roughness, the Leidenfrost point (LFP) temperature was especially sensitive to surface finish. The parametric effects of Weber number and surface temperature were consolidated into droplet impact regime maps for each of the three surface finishes. Aside from depicting the commonly known boiling curve regimes of film, transition and nucleate boiling, and thin film evaporation, these maps illustrate the complex liquid–solid interactions which occur during the lifetime of the impacting droplet within each of the boiling curve regimes, thus serving as an effective reference for future modeling of droplet heat transfer. Copyright © 1996 Elsevier Science Ltd.

1. INTRODUCTION

Recent advances in such areas as materials processing and microelectronics have established the need for both high heat dissipation rates and better spatial control over both heat flux and surface temperature. Recent studies have shown that spray cooling satisfies these requirements by controlling quench rate and material properties in heat treatable aluminum alloys [1–3], and enabling the dissipation of high heat fluxes from microelectronic and power devices [4]. However, while spray cooling shows promising results in both present and emerging technologies, much research is still needed to broaden the understanding of droplet impact and heat transfer mechanisms of sprays.

Quenching of heat treatable metallic parts has received considerable attention in the past decade from steel and aluminum producers for the automotive and aerospace industries, respectively. During a quench, the part experiences a relatively large and rapid temperature drop intended to suppress the precipitation of the alloying elements (solutes), enabling superior mechanical properties to be realized through subsequent aging. Accurate prediction of cooling rate and resulting material properties is highly desirable in order to reduce scrap and minimize costly trial-and-error production practices. In two recent studies, Hall and Mudawar [2, 3] used several spray heat transfer correlations developed for polished surfaces [5–7] to demonstrate how the thermal history and mechanical properties of spray quenched aluminum parts can be predicted with high accuracy.

One important spray cooling parameter whose effects remains poorly understood is surface roughness. Many of the parts produced in industry by extrusion, forging or casting acquire a rough surface texture. In a few investigations where it has been accounted for, surface roughness had a significant effect on, for example, the boiling characteristics of metallic surfaces [8] and the cooling history of spray-quenched parts [9]. Thus, accurate prediction and control of the quench history of metallic parts during heat treatment will demand an understanding of how surface finish influences the various boiling regimes during a quench.

1.1. *Surface roughness literature*

Past research has generally ignored the effects of surface roughness on droplet heat transfer; however, a few qualitative assessments can be cited. Surface roughness influence on sessile (stationary) droplet film boiling heat transfer was examined by Chandra and Aziz [10]. They measured significantly smaller droplet evaporation times when surface roughness features were at least the same order of magnitude as the thickness of the vapor layer beneath the droplet. Bradfeld [11] reported that surface features promote liquid–solid contact in film boiling. This suggests that rough surfaces require a thicker vapor layer between the droplet and the surface to sustain film boiling and, therefore, possess a higher LFP temperature. This was indeed observed by Cumo *et al.* [12], Baumeister *et*

† Author to whom correspondence should be addressed.

NOMENCLATURE

d_0	droplet diameter just prior to impact	Greek symbols	
Ra	arithmetic average surface roughness	ρ	density
T	temperature	σ	surface tension.
u_0	droplet velocity just prior to impact	Subscripts	
We	droplet Weber number ($\rho_f u_0^2 d_0/\sigma$).	f	liquid
		0	condition just prior to impact
		s	impact surface.

al. [13] and Nishio and Hirata [14]. More recently, Avedisian and Koplik [15] found that the LFP temperature for water droplets on porous ceramic surfaces increases with increasing porosity. They speculated that as porosity and, hence, vapor absorption in the surface pores increase, a larger surface superheat is required to maintain a sufficiently thick vapor layer and, therefore, sustain film boiling.

Only a few investigators have explored the effects of roughness on droplet impact and their findings are only qualitative in nature. Engel [16], for example, observed that surface roughness promotes droplet breakup, and Ganic and Rohsenow [17] reported surface roughness enhances liquid–solid contact in dispersed droplet flow and hence, increases film boiling heat transfer. In a more application specific investigation, Bernardin and Mudawar [9] demonstrated that increased surface roughness due to oxidation and pitting on aluminum samples during repeated heat-quench cycles has a measurable influence on spray cooling rate.

1.2. *Focus of investigation*

To better understand the mechanisms of spray heat transfer, an investigation into single droplet impact and heat transfer was recently undertaken by the authors [18] to establish a consolidated means of describing impact behavior on polished surfaces. High speed photography and heat transfer measurements were used to construct droplet impact regime maps, which identified the spreading and heat transfer mechanisms of impinging droplets over broad ranges of surface temperature and impact velocity. The effect of impact velocity, u_0, was explored with the aid of the droplet Weber number, We, defined as the ratio of droplet inertia to surface tension forces.

$$We = \frac{\rho_f u_0^2 d_0}{\sigma}. \quad (1)$$

The objective of the present study is to further the understanding of droplet impact on heated surfaces using the photographic and heat transfer measurement techniques developed in ref. [18] for polished surfaces, but with special emphasis on the effects of surface roughness. This objective is accomplished in the following three tasks.

(1) The previous photographic investigation of single droplet impact [18] is extended to include surface roughness effects in addition to variations in droplet Weber number and surface temperature.

(2) Heat transfer measurements for a droplet stream impinging upon a heated surface are used to identify boiling curve regimes (film, transition and nucleate boiling, and thin film evaporation) and determine the CHF and LFP temperatures.

(3) Droplet impact regime maps are constructed to capture the complex droplet deformations and transient heat transfer mechanisms within each boiling regime for different surface finishes.

2. EXPERIMENTAL APPARATUS AND PROCEDURE

Figure 1(a) shows a schematic of the apparatus employed to study the impact of single droplets and droplet streams on heated surfaces. A fluid delivery system consisting of a reservoir, a magnetically driven centrifugal pump and a needle valve, produced repeatable droplets from a 0.58 mm (0.023 in) hypodermic needle situated directly above the impact surface. Only deionized water (which was frequently replaced) was used in the system to prevent any changes to fluid properties due to contamination. A more detailed discussion of this apparatus can be found in ref. [18].

Two types of heater modules were used in the present study. The first was employed in heat transfer measurements aimed at capturing the general boiling curve regimes (film, transition and nucleate boiling, and thin film evaporation) and boundary temperatures (LFP and CHF) between these regimes when quenching a hot surface by a stream of droplets. The second heater module was used in a photographic study of single droplet impact on a heated surface to capture the detailed liquid–solid interactions and associated heat transfer mechanisms occurring within each boiling regime.

2.1. *Heat transfer measurements*

The first heater module, Fig. 1(b), consisted of a thin copper disk mounted in a larger insulating G-7

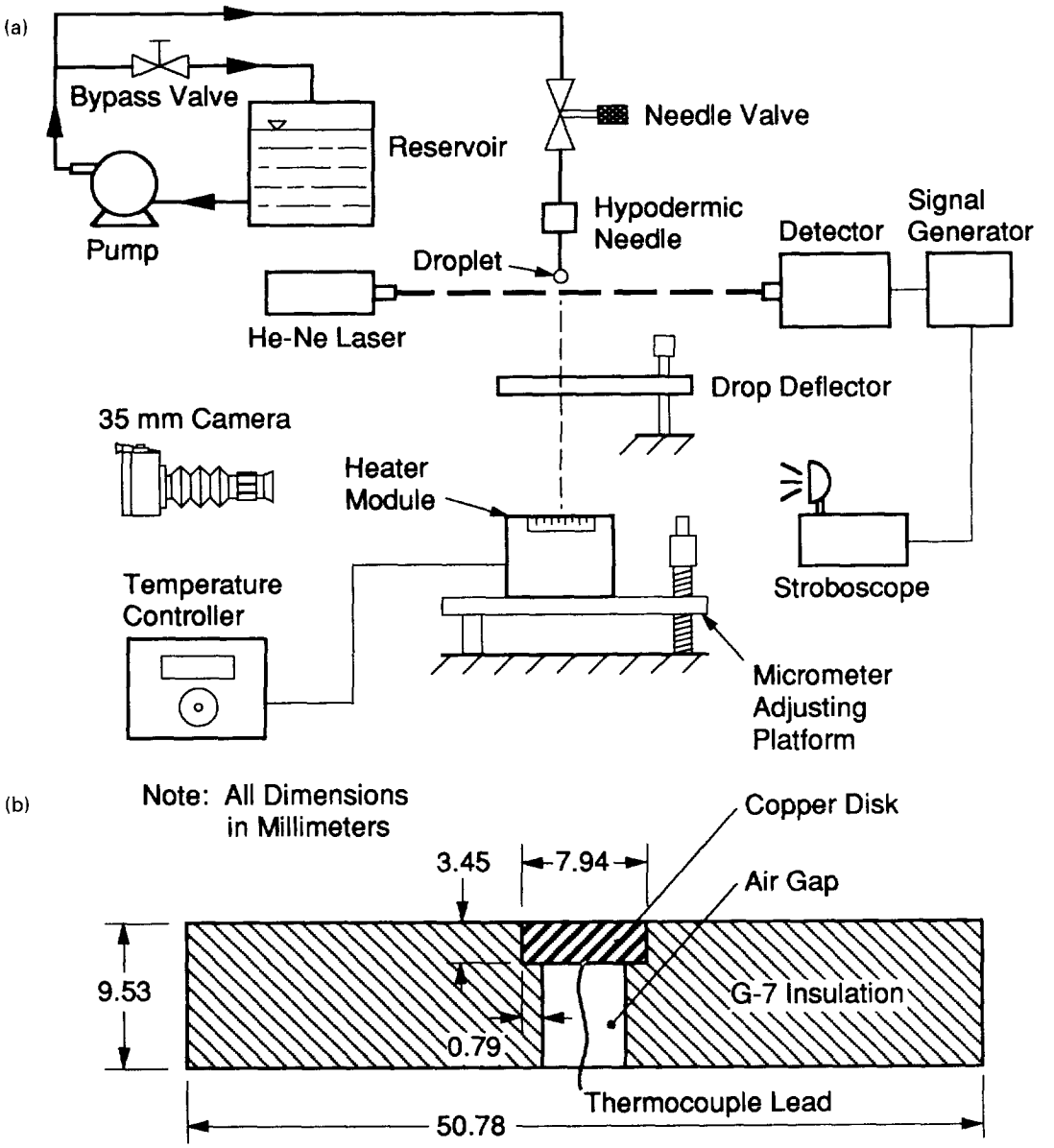

Fig. 1. Schematics of (a) test apparatus and (b) droplet impact module used in heat transfer measurements.

fiberglass disk. The copper disk was made thin enough to ensure isothermal conditions at each instant during the quench. A Chromel–Alumel (type K) thermocouple mounted to the back of the disk was connected to a computer-driven Keithley 500 data acquisition system to record the *transient* cooling history. Prior to impact by a droplet stream, the disk was preheated using an Unger 1095 heat gun.

Three surface finishes, polished, particle blasted and rough sanded, with respective arithmetic average surface roughness values of 97, 970 and 2960 nm were applied to different disks. Figure 2 shows scanning electron microscope (SEM) images for the three surfaces along with the respective surface height distributions measured with a surface contact profilometer. Surface features on the polished disk were the smallest, mostly below 1 μm, while the particle blasted and rough sanded surfaces possessed features as large as 5 and 15 μm, respectively. Despite having a relatively smaller arithmetic average surface roughness, Fig. 2(b) shows the particle blasted surface possessed nucleation features superior to those on the rough sanded surface, Fig. 2(c).

The heat transfer measurements commenced by throttling the flow to generate a steady stream of droplets with the desired Weber number at a frequency of 150 droplets min^{-1} (dpm). A deflector plate was positioned to shelter the disk, during which time the heat gun was directed upon the disk. The deflector plate was removed the instant the disk reached 280°C;

the data acquisition system began recording the disk temperature every 20 ms until it fell below 100°C. A computer code based on the assumption of lumped capacitance was used to convert the recorded temperature–time cooling curve to a boiling curve, from which the temperatures corresponding to CHF and LFP were determined. This procedure was repeated for $We = 20$, 60 and 220 for each of the three surface finishes. To ensure reproducibility, six tests were conducted for each set of operating conditions.

2.2. *Photographic methods*

The second of the two heater modules, shown in Fig. 1(a), consisted of a rectangular aluminum block which was mounted in an insulating G-7 fiberglass plastic shell. The three surface finishes described in Fig. 2 were applied to different aluminum blocks. The desired steady state impact surface temperature was maintained by an Ogden Type 33 temperature controller, which manipulated power input to a cartridge heater inserted in the aluminum block in response to a type K thermocouple embedded just beneath the impact surface. The heater module was situated on a vertical micrometer translation platform to fine tune impact surface elevation and the corresponding strobe delay time for the droplet detector system described below.

To acquire the information necessary for constructing the droplet impact regime maps, a Kodak EktaPro 1000 motion analyzer, with a speed of 1000 frames s^{-1} or 6000 partial frames s^{-1}, was used along with bellows, a 200 mm zoom lens and a high intensity light source. The video segments provided a continuous record of the impact of a single droplet, alas with relatively inferior resolution. High resolution photos of crucial instances of the impact were possible with the aid of a 35 mm camera equipped with bellows and a 200 mm zoom lens, a Kodak P3200 high resolution film and a General Radio 1538-A strobe. The strobe was set to produce a high intensity, short-pulse flash controlled by the droplet detector system illustrated in Fig. 1(a). The operation of this system was as follows. Droplet fall from the hypodermic needle momentarily shaded a He–Ne laser beam directed upon a photoresistor in the detector's circuit. The photoresistor tripped a second circuit, passing a 1 volt pulse to a signal generator. The signal generator then passed a square pulse to trigger the strobe. The delay time from the instant of droplet fall to the instant of the flash was set by trial and error to coincide with the commencement of impact by varying the width of the signal generator's square wave. Subsequent stages of the impact, usually separated by milliseconds, were captured by decreasing the frequency of the square

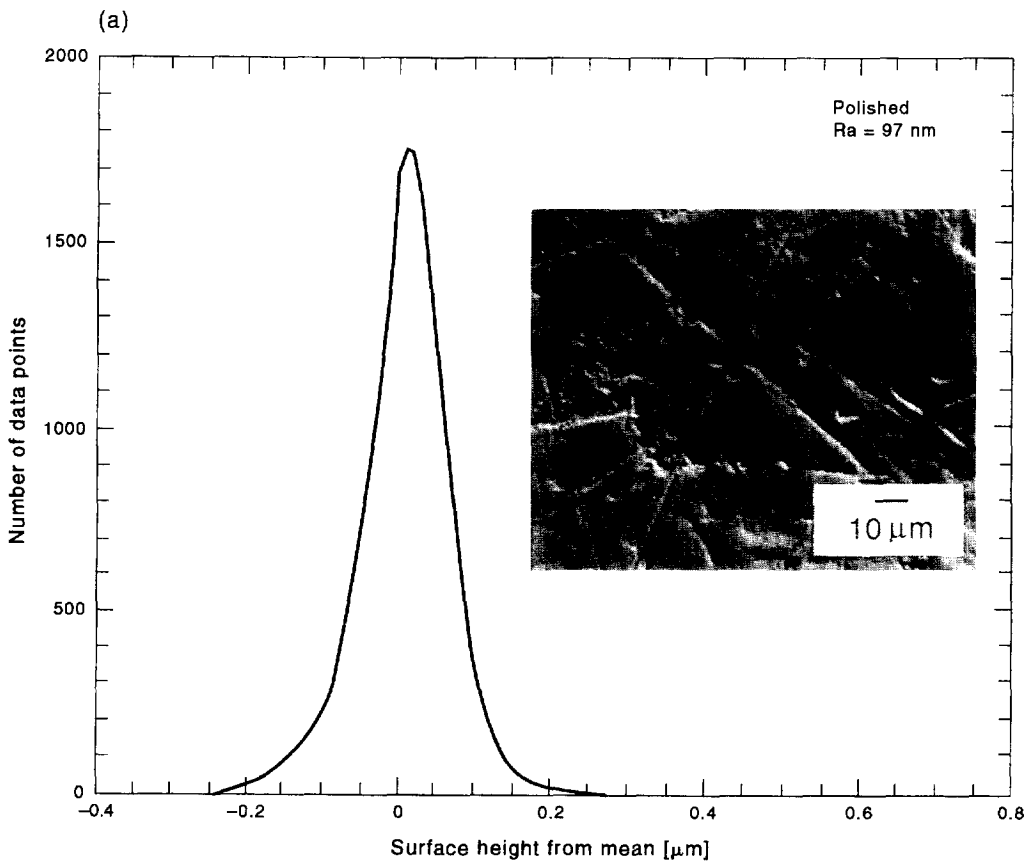

Fig. 2. Scanning electron microscope images and surface height distributions for copper disks with (a) polished, (b) particle blasted and (c) rough sanded finishes. (*Continued opposite.*)

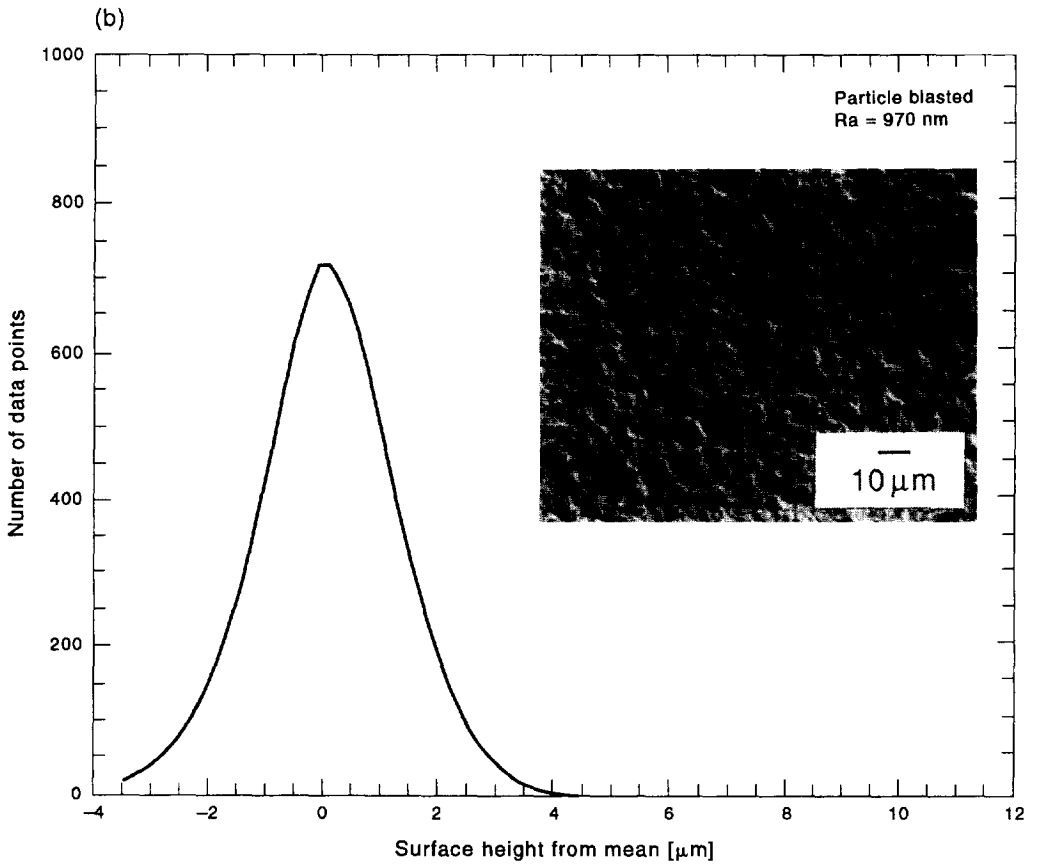

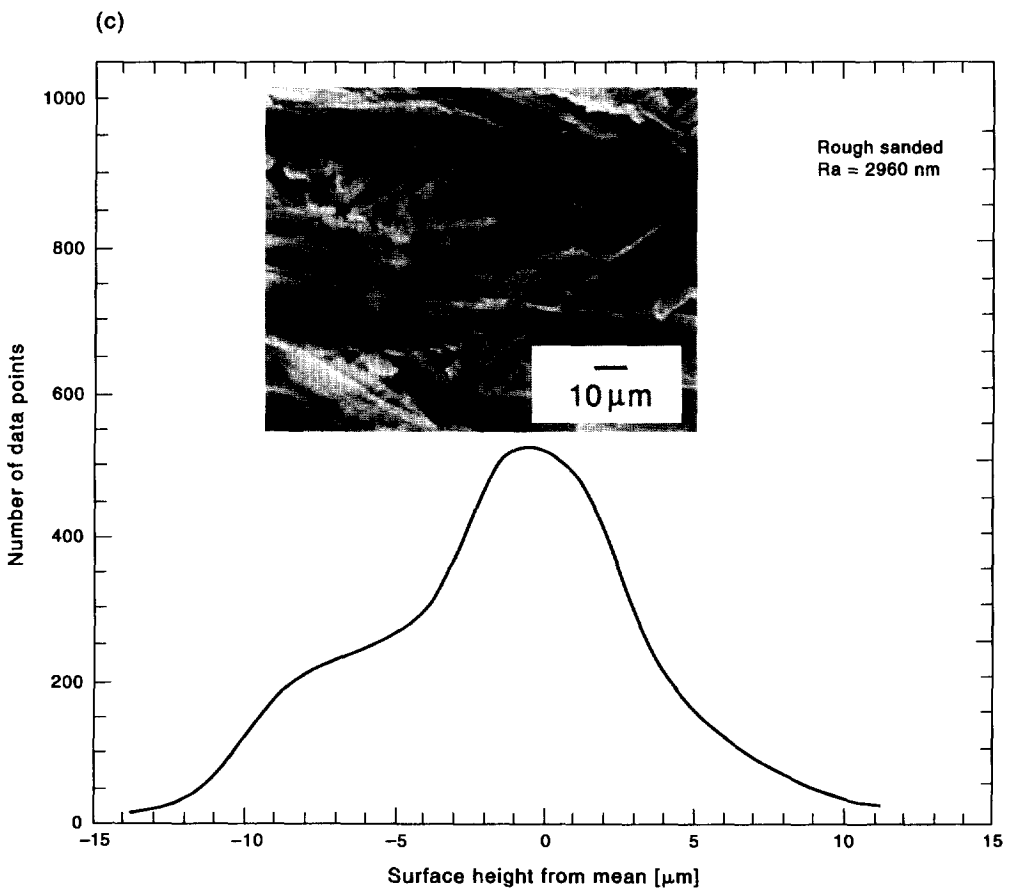

Fig. 2. (*Continued.*)

pulse from the signal generator, and hence increasing the delay time of the strobe. Additional details concerning the design and operation of the droplet detector system can be found in ref. [18].

The photographic study included variations in droplet velocity, surface temperature and surface roughness. The high speed video system was used to record several droplet impacts at 20°C surface temperature decrements from 280 down to 100°C and droplet Weber numbers of 20, 60 and 220. These Weber numbers correspond to droplet velocities of 0.70, 1.21 and 2.34 m s^{-1}, respectively, and a nearly constant droplet diameter of 3.0 mm. Hatta *et al.* [19] have shown that the correlations for the maximum spreading diameter and residence time developed for 2 to 3 mm water droplets on smooth surfaces are equally valid for 0.3–0.6 mm droplets.

The 35 mm camera was used in conjunction with the droplet detector mechanism to obtain top and side view photographs corresponding to several stages of the impact for surface temperatures of 125 and 280°C, and a Weber number of 220 for each of the three surface finishes. These two temperatures were chosen to represent the two extreme behaviors of nucleate boiling and film boiling, respectively. Only a single Weber number was examined, since the effects of Weber number were reported in a previous study [18] and because this relatively high Weber number is more representative of conditions found in spray cooling. The still photographs were taken in a dark laboratory with the camera shutter open several seconds prior to the impact. Several photographs were taken for each set of operating conditions before adjusting the time delay to capture a later stage of the impact. The individual photos were pieced together with the aid of the high speed video segments to construct the complete history of the impact. Each test condition was captured several times on high-speed video tape and carefully analyzed to ensure impact reproducibility and thus justify piecing together photos of different droplets.

3. EXPERIMENTAL RESULTS AND DISCUSSION

The experimental results are presented in two sections. First, the heat transfer results are presented to show how surface roughness influences the various boiling regimes, as well as the CHF and LFP temperatures which separate the transition boiling regime from the nucleate and film boiling regimes, respectively. Next, droplet impact regime maps captured from high speed video segments will be presented to summarize the complex liquid–solid interactions occurring within each boiling regime for different surface roughnesses. Still photo sequences are also provided for the highest Weber number, 220, to help clarify the impact characteristics indicated in the regime maps.

3.1. *Heat transfer measurements*

Heat transfer measurements from the small copper disk to an impinging stream of water droplets were used to determine the temperatures corresponding to CHF and LFP for the various Weber numbers and surface finishes. Transient cooling curves and corresponding boiling curves for the polished, particle blasted, and rough sanded surfaces are shown in Figs. 3–5 for $We = 20$, 60 and 220, respectively. The boiling curves are plotted with respect to surface-to-fluid temperature difference, $T_s - T_f$, where $T_f = 23$°C. Each curve is representative of six data sets taken to ensure reproducibility. The fluctuations in these boiling curves are the result of periodic impact by the droplets, as explained in ref. [18].

The cooling and boiling curves in Figs. 3–5 reveal that the impinging droplet heat transfer characteristics are influenced to varying degrees by surface roughness. First, the heat fluxes in the film boiling regime are relatively small and do not show a strong dependence on surface roughness for any of the Weber numbers tested. Heat flux in the transition boiling regime can be loosely divided into two roughness dependent regions. In the upper portion of the transition boiling regime, corresponding to surface temperatures above 150°C, the heat flux is highest for the polished surface, followed, respectively, by the particle blasted and rough sanded surfaces. In the portion of the transition boiling regime below 150°C and the entire nucleate boiling regime, the heat flux is highest for the particle blasted surface, followed, respectively, by the rough sanded and polished surfaces because of the strong influence of liquid–solid contact and nucleation site density in these regimes. Interestingly, the dependence of heat flux on surface roughness over the entire transition and nucleate boiling regimes is consistent with the pool boiling results by Corty and Foust [20] and Berenson [21]. The boiling curves of Figs. 3–5 reveal a decreasing surface roughness dependence across the transition and nucleate boiling regimes with increasing Weber number.

Figure 6 displays CHF and LFP temperatures corresponding to the different droplet Weber numbers and surface furnishes, obtained from boiling curves similar to those of Figs. 3–5. These temperatures were averaged from six data sets with an interpolation uncertainty of ± 10°C. Three shaded maximum error bands extend 10°C above the highest temperature and 10°C below the lowest temperature for LFP for the polished surface, LFP for the particle blasted and rough sanded surface, and CHF for all three surfaces. Both the CHF and LFP temperatures seem fairly insensitive to droplet impact velocity over the tested range. The CHF temperature of approximately 130°C also appears to be insensitive to surface roughness. On the other hand, LFP temperature shows appreciable sensitivity to surface roughness, 225°C for the polished surface and about 40°C less for both the particle blasted and rough sanded surfaces.

Figure 6, as well as the boiling curves in Figs. 3–5,

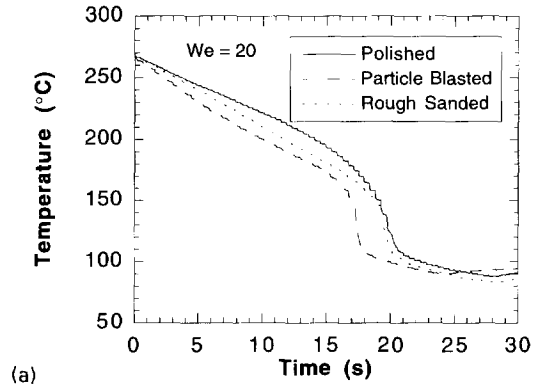

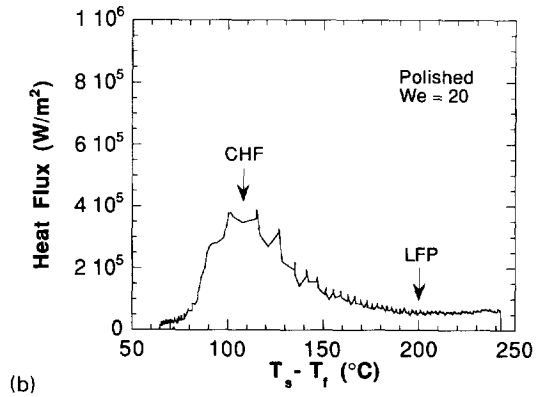

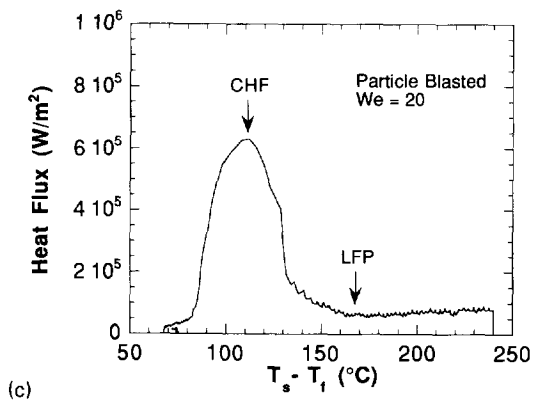

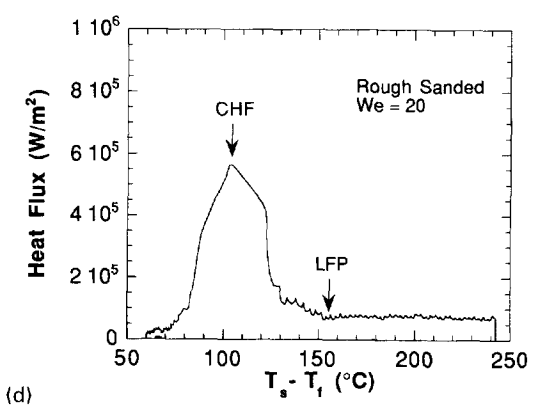

Fig. 3. (a) Cooling curves and corresponding boiling curves for water droplets with a $We = 20$ striking a copper disk with a (b) polished, (c) particle blasted and (d) rough sanded surface.

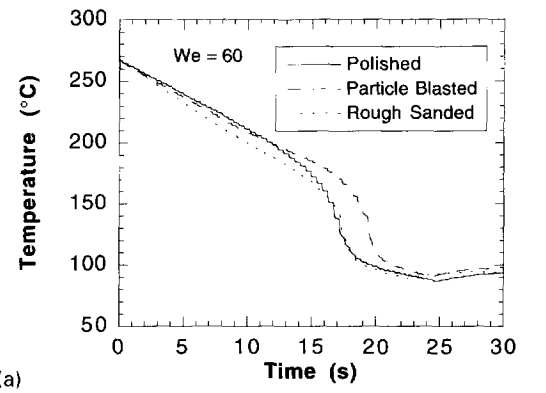

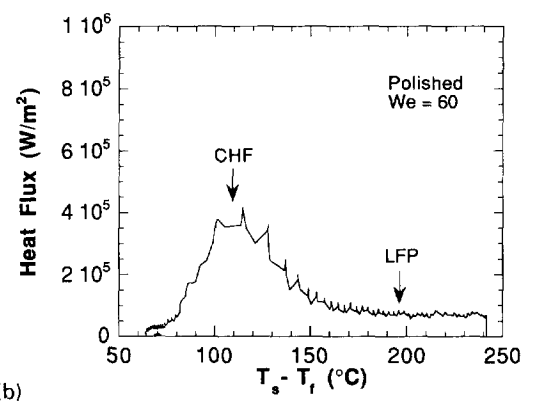

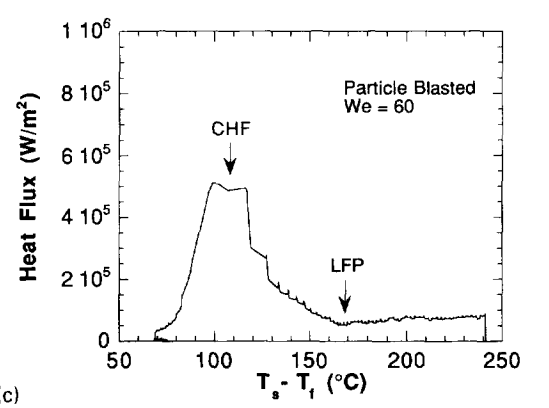

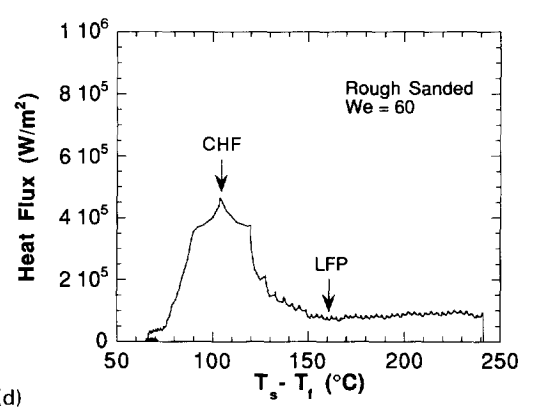

Fig. 4. (a) Cooling curves and corresponding boiling curves for water droplets with a $We = 60$ striking a copper disk with a (b) polished, (c) particle blasted and (d) rough sanded surface.

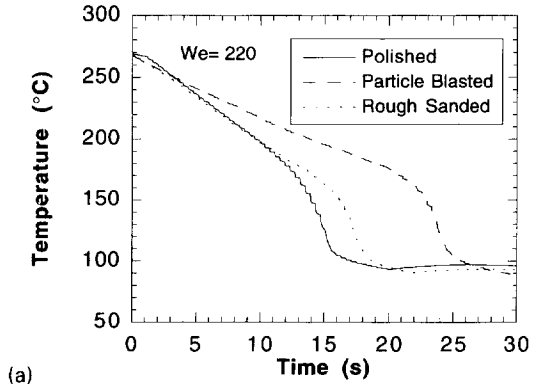

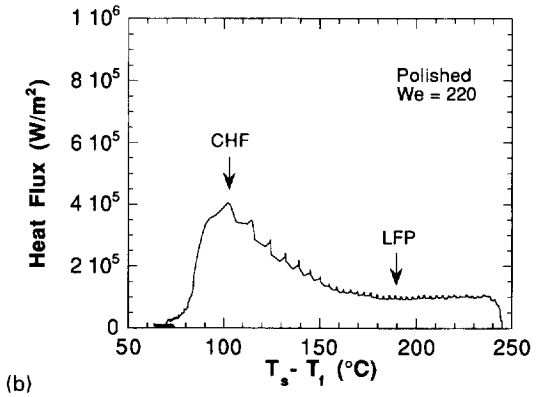

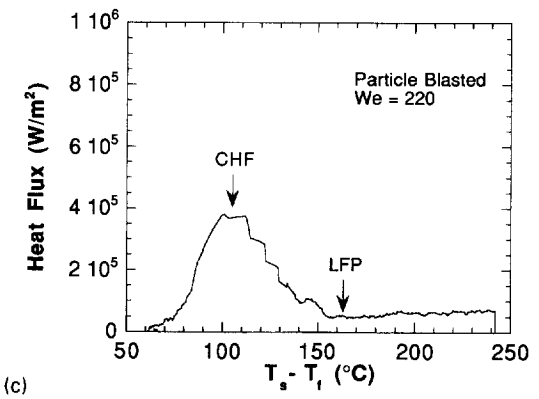

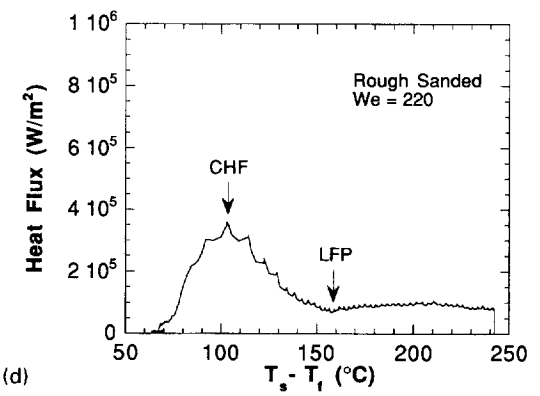

Fig. 5. (a) Cooling curves and corresponding boiling curves for water droplets with a $We = 220$ striking a copper disk with a (b) polished, (c) particle blasted and (d) rough sanded surface.

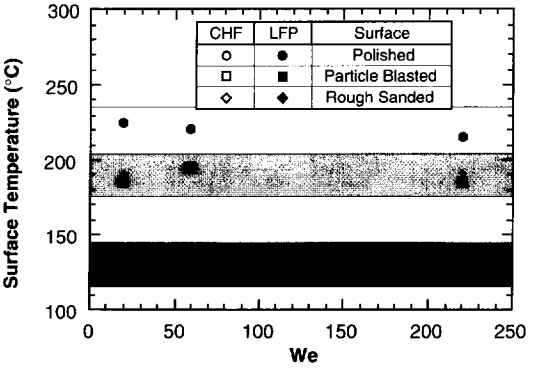

Fig. 6. Surface temperatures corresponding to CHF and LFP for surfaces of different roughnesses.

reveal that the CHF temperature is nearly independent of droplet impact velocity and surface finish. The LFP temperature, however, while also fairly insensitive to droplet velocity (for the tested range), decreases with increasing surface roughness. Berenson [21] and Tong [22] reported that pool boiling heat flux at CHF and LFP are insensitive to surface roughness. The pool boiling experimental data of ref. [21] show, however, that the *temperature* corresponding to CHF decreases with increasing roughness while the LFP temperature is insensitive to surface roughness. Previous sessile droplet studies [11–14] have shown that LFP temperature increases with increasing roughness. This apparent contradiction to the results reported here may be the result of fundamental differences in heat transfer mechanisms between pool boiling, sessile droplets and impinging droplets.

The differences in the influence of surface roughness on the LFP temperature for sessile vs impinging droplets is believed to be related to the combined effect of surface features and pressure beneath the droplet. For sessile droplets, the surface features play a dominant role in penetrating the vapor layer beneath the droplet, yielding higher LFP temperatures for rougher surfaces. Impinging droplets, on the other hand, are also strongly influenced by the large stagnation pressure resulting from the impact. It has been reported that the LFP temperature increases with increasing pressure, both ambient [23–25] and as a result of the impact [26, 27]. The impact causes the droplet to spread out into a thin liquid film. As the photographic sequences will later reveal, the film is far more stable on the polished surface than on the rougher surfaces. In fact, the protruding surface features tend to violently rupture the film, greatly reducing the pressure beneath the spreading droplet relative to a polished surface. Hence, the LFP temperature is greater for a droplet impinging on a polished than a rough surface.

3.2. *Impact regime maps*

Impact regime maps are used to summarize droplet impact behavior and associated heat transfer regimes for different Weber numbers and three surface rough-

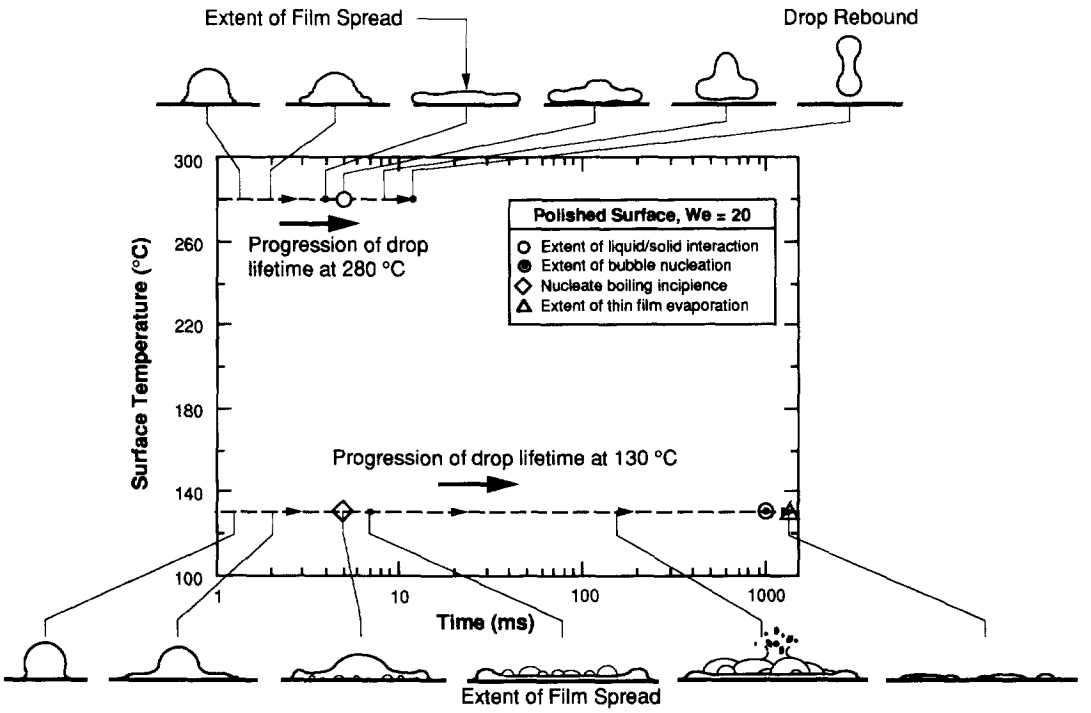

Fig. 7. Schematic aid for reading droplet regime maps.

nesses. Figure 7 serves as a guide to reading a typical regime map, using droplet impact schematics corresponding to a polished surface and a droplet Weber number of 20 as an example. For a given surface temperature (ordinate), the impact history of the droplet is described by following a horizontal line across the regime map corresponding to the lifetime of the droplet (abscissa). At various times along this line, distinct impact characteristics are represented by two types of symbols. Small solid circles are used to describe the fluid impact behavior such as the maximum extent of film spread, droplet rebound and complete droplet breakup. Boundaries of the various intermediate heat transfer mechanisms, on the other hand, are denoted by open symbols listed in the map legend. In addition to the symbols, schematics of the impact for two droplets at surface temperatures of 280 and 125°C are provided to further illustrate the symbol notations. For example, at a surface temperature of 280°C, the maximum extent of the spreading film is identified by a small solid circle while, at a later instant, the extent of liquid–solid interaction and associated heat transfer is represented by a large open circle. Finally, the rebound of the droplet is identified by another small solid circle. For a surface temperature of 125°C, the impact characteristics are characteristically different from those at 280°C, as noted by the different deformation diagrams and two orders of magnitude difference between droplet lifetimes. In addition to describing the fluid and heat transfer mechanisms of individual droplets, each of the impact regime maps given in the next section will display the boiling regimes (film, transition and nucleate boiling and thin film evaporation) and the boundary temperatures (CHF and LFP) between these regimes, identified from the heat transfer measurements described in the previous section.

Low Weber number results. Figure 8(a–c) presents droplet regime maps for the three surface finishes and a Weber number of 20. Each map displays the dominant droplet impact characteristics associated with each of the boiling curve regimes (indicated to the right of each map). For this low Weber number case, where surface tension forces play a relatively important role in resisting droplet breakup, the maps reveal similarities in impact behavior between the different surfaces.

Within the entire film boiling regime of each map, the droplet spreads into a stable liquid film in the first 4 or 5 ms of impact, which then recoils into a rebounding droplet after 8–13 ms from impact. The protruding features on the particle blasted and rough sanded surfaces preserve liquid–solid contact until rebound. In the absence of similar features on the polished surface, a thin vapor layer which develops beneath the spreading droplet prevents liquid contact with the surface. The LFP temperature of 225°C (determined from the heat temperature measurements described in the previous section) for the polished surface is notably higher than the 190°C for both the particle blasted and rough sanded surfaces.

Some of the impact characteristics of the film boiling regime extend down to surface temperatures within the transition boiling regime. However, increased surface wetting in the latter regime prevents complete droplet rebound; only a portion of the liquid

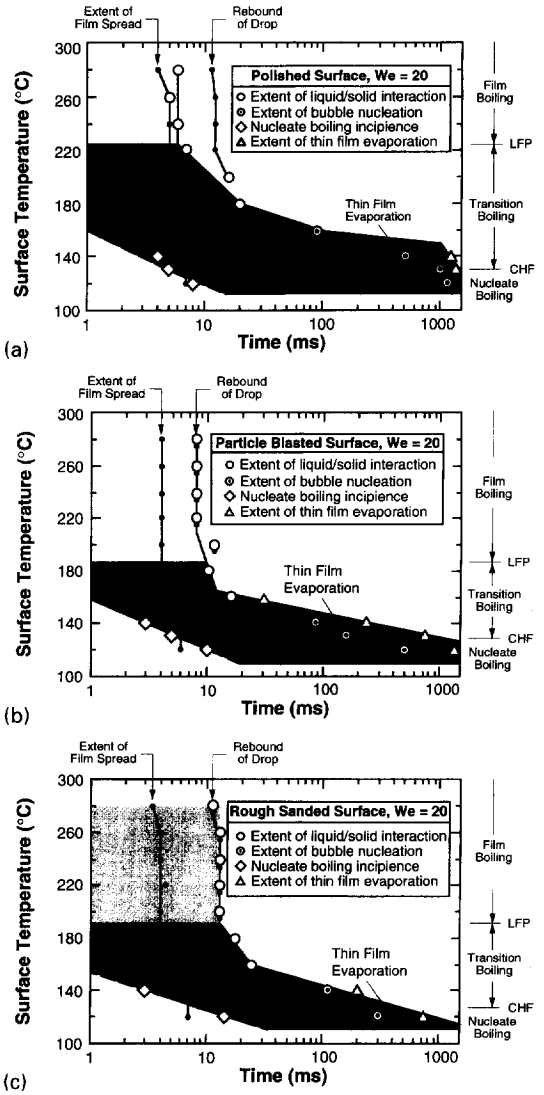

Fig. 8. Droplet impact regime maps for $We = 20$ and (a) polished, (b) particle blasted and (c) rough sanded surfaces.

is expelled from the surface during impact. The liquid remaining in contact with the surface experiences intense boiling followed, for lower transition boiling temperatures, by thin film evaporation. For each of the three surfaces, boiling in the range of 160–130°C (lower half of the transition boiling regime) is delayed during the initial stage of impact, as noted by the dashed line corresponding to boiling incipience. While the incipience condition is similar for all three surfaces, the extent of the subsequent boiling process is highly dependent upon the surface finish. Figure 8(a–c) reveals that the droplet lifetime decreases with increasing surface roughness, suggesting boiling is enhanced by the more abundant nucleation cavities on the rougher surfaces. Unlike the LFP temperature, which is appreciably higher for the polished surface, the CHF temperature (lower boundary of the transition boiling regime) is about the same, 130°C, irrespective of surface roughness.

Below CHF is the nucleate boiling regime, which is characterized by a complete spreading of the impinging drop, followed by vigorous boiling, and, finally, thin film evaporation. Extended droplet lifetimes in the nucleate boiling regime compared to those in the lower temperature range of the transition boiling regime seem to be the cumulative effect of complete spreading of the droplet prior to boiling incipience, drastic reduction in liquid ejection from the surface during the boiling process, and film evaporation making up a larger fraction of the droplet lifetime as less superheat is available for bubble nucleation and growth. As with the transition boiling regime, enhanced nucleation on the rougher surfaces decreases droplet lifetime.

Intermediate Weber number results. Figure 9(a–c) shows the impact regime maps for $We = 60$ for the polished, particle blasted and rough sanded surfaces, respectively. Compared to $We = 20$, the increased droplet velocity weakens the ability of the surface

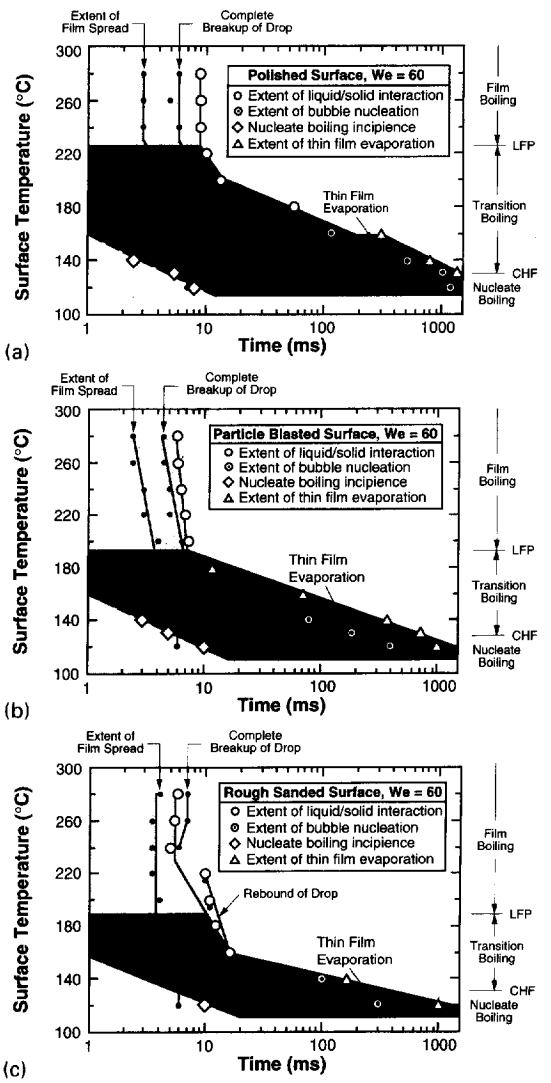

Fig. 9. Droplet impact regime maps for $We = 60$ and (a) polished, (b) particle blasted and (c) rough sanded surfaces.

tension forces to restore liquid continuum following impact. As with the lower Weber number case, the regime maps in Fig. 9(a–c) display several similarities, as well as characteristic differences, for the different surface roughnesses.

In the film boiling regime, the spreading liquid film quickly becomes disturbed and breaks into a large number of small droplets which rebound away from the surface in less than 10 ms. As with the lower Weber number case, the LFP temperature is 225°C for the polished surface, roughly 40°C higher than the two rougher surfaces.

Variations in the wetting, fluid flow, and vapor bubble formation characteristics caused by the unique surface roughness features are responsible for the observed differences in droplet lifetime depicted in Fig 9(a–c). For the polished surface, the impact characteristics in the upper half of the transition regime are similar to those described above for film boiling. Below 160°C, boiling incipience is delayed a few milliseconds, after which intense boiling ensues, which is then followed by thin film evaporation. For the particle blasted surface, the impact characteristics vary gradually from droplet breakup to a nearly complete surface adherence as the surface temperature is decreased in the transition regime. Most notable for the particle blasted surface in transition boiling is the extended thin film evaporation. For the rough sanded surface, the impact characteristics are similar to those described in Fig. 8(c) for $We = 20$. A CHF temperature of 130°C is again independent of surface roughness. Below CHF, nucleate boiling behavior for the three surface finishes is nearly identical to that described earlier for the lower Weber number droplets of Fig. 8.

High Weber number results. Figure 10(a–c) displays the impact regime maps for droplets impinging upon the polished, particle blasted and rough sanded surfaces, respectively, with $We = 220$. These maps display shorter spreading times and more violent breakups as compared to the maps presented earlier for the two lower Weber numbers. However, the major influences of surface roughness on droplet impact behavior are still evident for $We = 220$.

Within the film boiling regime, the impinging droplets experience quicker and more violent breakup on the rough sanded and particle blasted surfaces than on the polished surface. The short, but similar, lifetimes displayed in these maps suggest, while influencing the spreading and breakup of the liquid film, that the surface roughness has a relatively mild influence on heat transfer in film boiling. However, the influence of surface roughness is realized at the LFP temperature. The polished surface has a LFP temperature of 220°C, approximately 40°C higher than that for the rough sanded and particle blasted surfaces.

The impact behavior within the transition boiling regime is drastically different for the different surfaces, as evidenced by the different temperatures and durations of droplet deformation characteristics corresponding to the different surfaces. The impact behavior for each surface changes throughout the transition regime, as enhanced liquid–solid contact with decreasing surface temperature increases the rate of conversion of liquid into vapor and the overall droplet lifetime. For each surface, a boiling incipience delay and thin film evaporation mark the early and late stages, respectively, of the impact for temperatures nearing the low end of the transition regime.

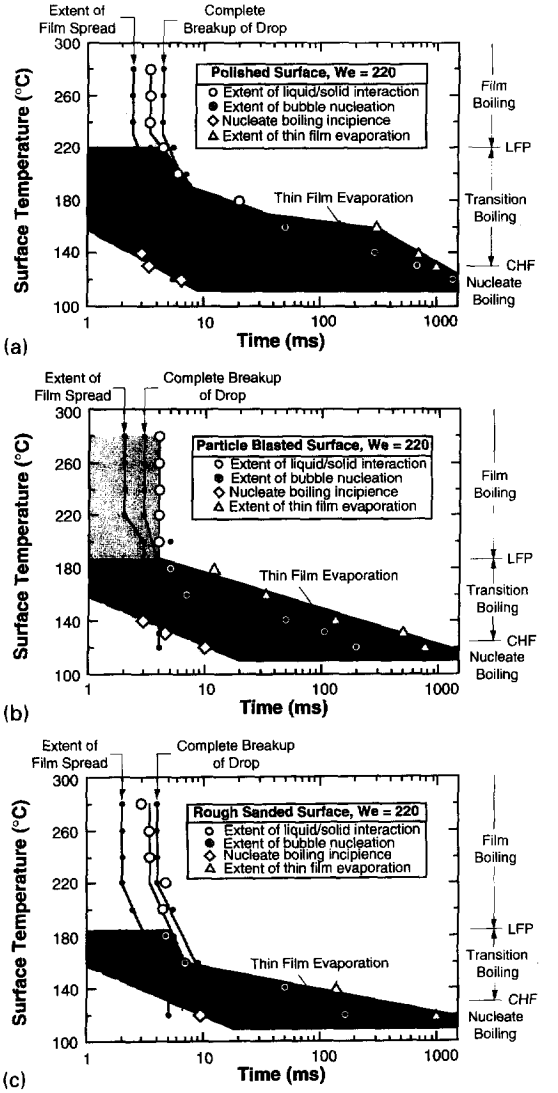

Fig. 10. Droplet impact regime maps for $We = 220$ and (a) polished, (b) particle blasted and (c) rough sanded surfaces.

The impact characteristics are generally similar for each surface in the nucleate boiling regime, except for a systematic decrease in droplet lifetime with increasing roughness, possibly due to the increased nucleation site density on the rougher surfaces. The impact begins on each surface with a film spread, followed by a few millisecond boiling incipience delay, vigorous boiling, and finally, thin film evaporation.

To further illustrate the impact of single droplets described in the regime maps for the different surface

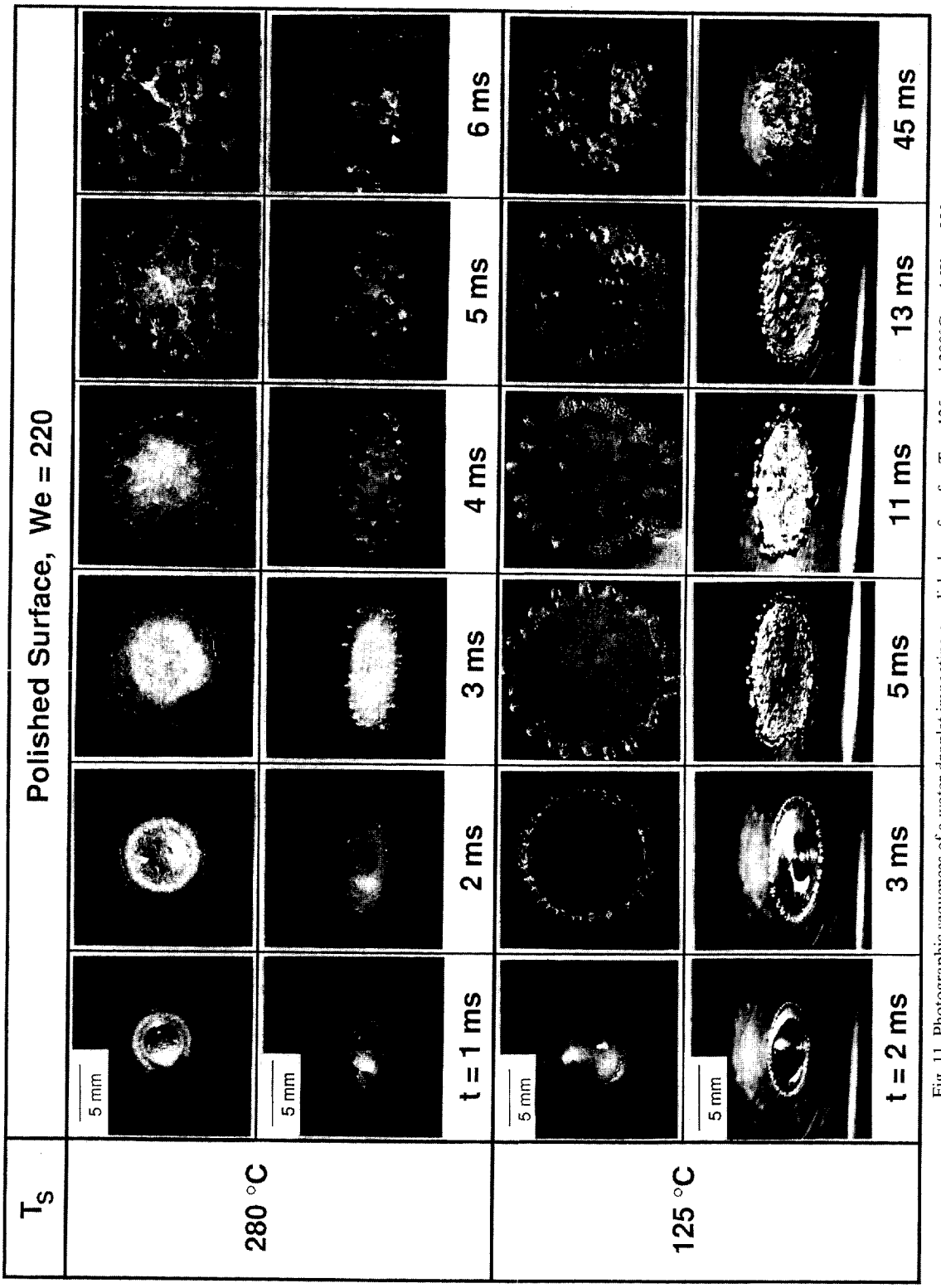

Fig. 11. Photographic sequences of a water droplet impacting a polished surface for $T_s = 125$ and 280°C and $We = 220$.

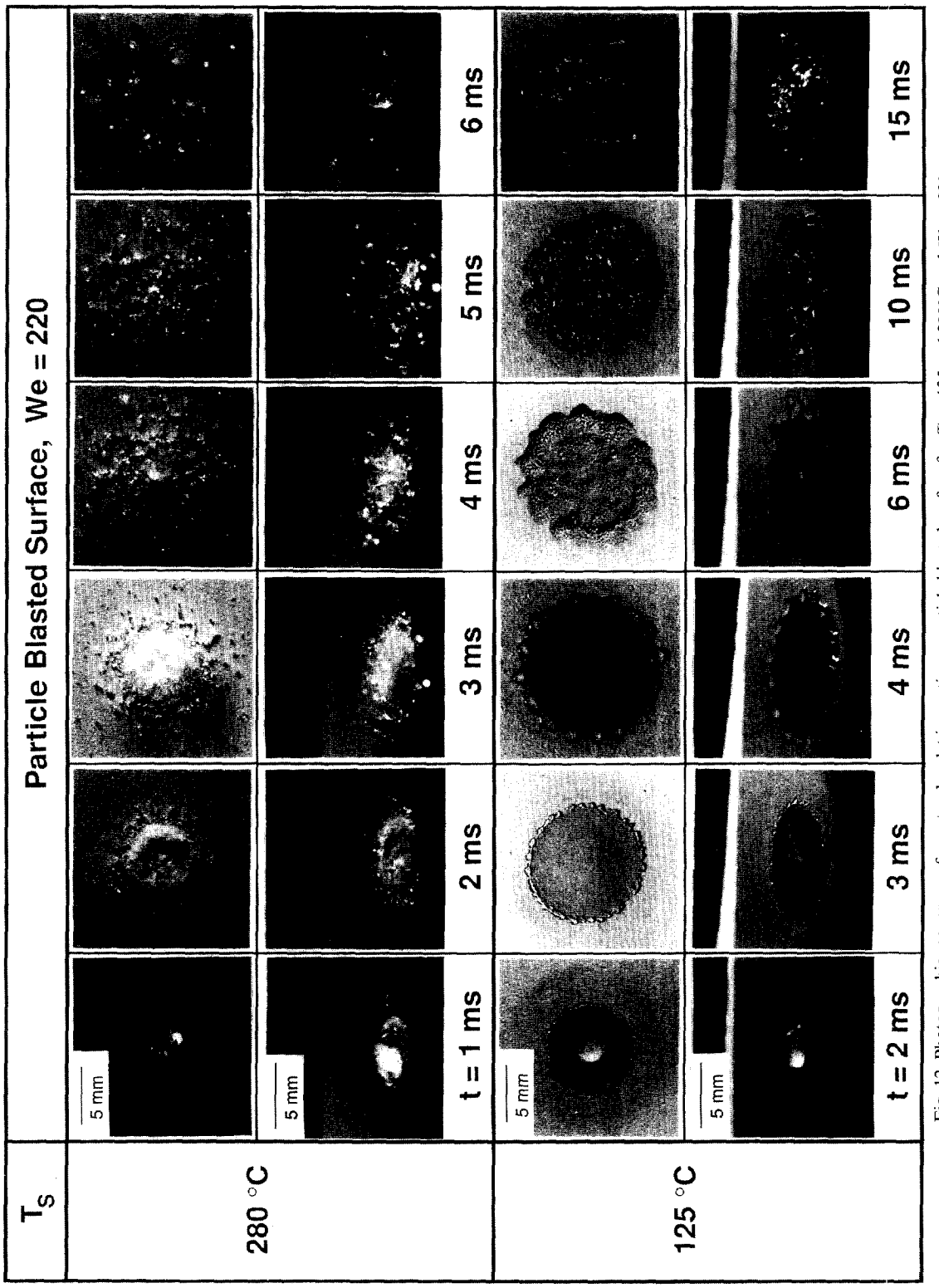

Fig. 12. Photographic sequences of a water droplet impacting a particle blasted surface for $T_s = 125$ and 280°C and $We = 220$.

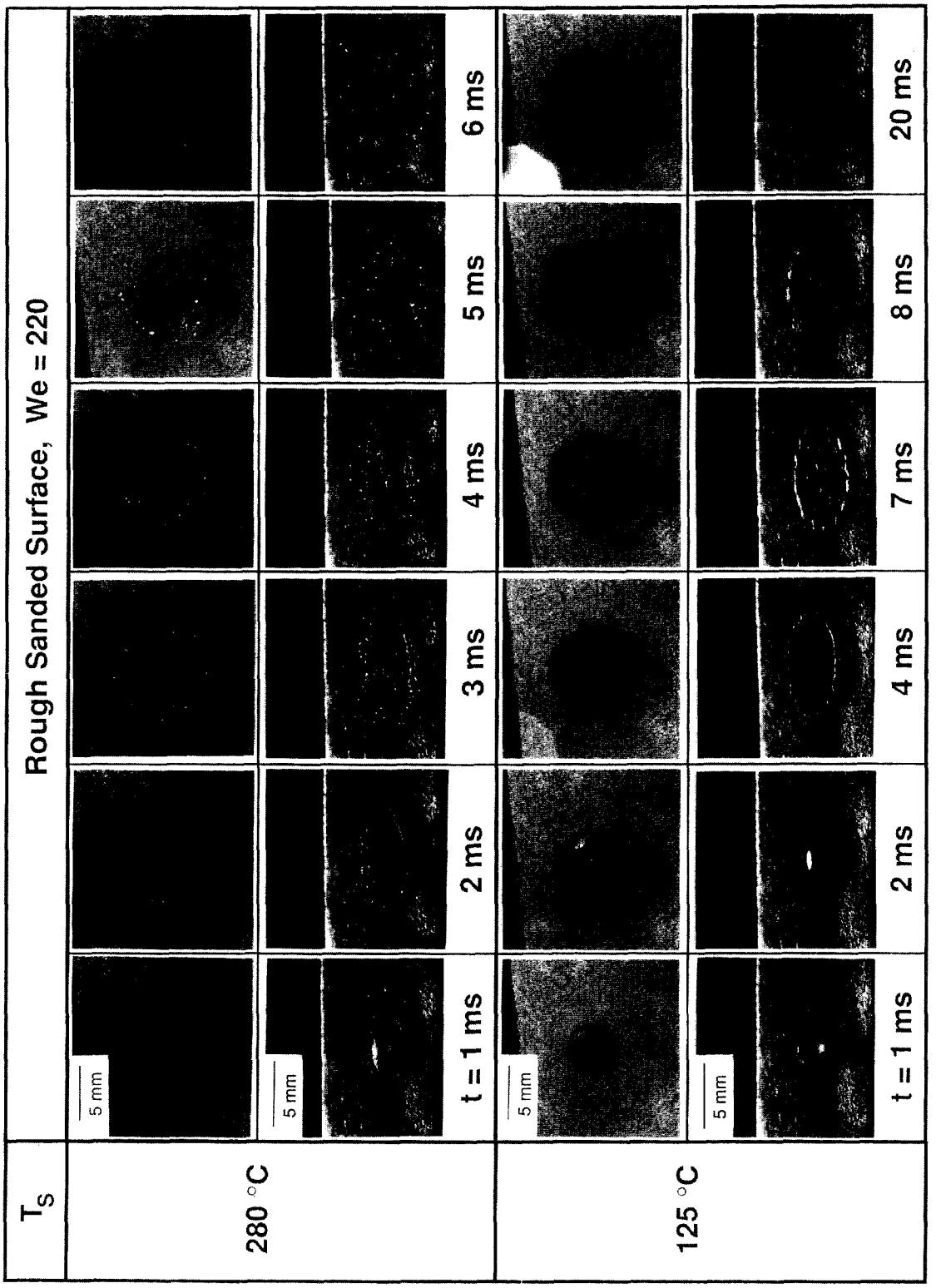

Fig. 13. Photographic sequences of a water droplet impacting a rough sanded surface for $T_s = 125$ and 280°C and $We = 220$.

finishes, side and top view still photos were taken for $We = 220$ and surface temperatures of 125°C and 280°C. These are presented in Figs. 11–13 for the polished, particle blasted and sanded surfaces, respectively. For $T_s = 280$°C (film boiling regime), the photo sequence in Fig. 11 shows the droplet spreads into a disturbed, but intact liquid film. Interfacial disturbances on the film underside caused by a rapid change of phase causes the eventual breakup of the film within 6 ms of impact. In contrast, Figs. 12 and 13 show an intact liquid film never fully develops on the two rough surfaces, and breakup into small droplets occurs within the first 4 ms of impact. Apparently, the surface features effectively penetrate the vapor layer disrupting the radial film flow; the more rapid vapor production further accelerates the breakup of the liquid film. This is especially evident at the leading edge of the spreading film on the two rough surfaces, Figs. 12 and 13. These observations are consistent with the impact regime maps of Fig. 10 which reveal a faster breakup of droplets on the rough surfaces in the film boiling regime. The influence of the surface features is especially evident in Fig. 10(b) for the particle blasted surface on which liquid–solid interactions persist, even after complete breakup of the droplet. It is speculated that droplet disintegration and enhanced liquid–solid contact are competing effects in film boiling heat transfer. As the heat transfer measurements in the previous section have shown, film boiling heat flux is not strongly influenced by surface roughness.

At the lower temperature of 125°C (nucleate boiling regime), the impact history for each of the three surfaces begins with an intact liquid film spread, followed by a delay period before nucleate boiling ensues. A greater number of active nucleation sites on the two rougher surfaces than on the polished surface leads to quicker and more vigorous boiling, which is evident when comparing the bubble formations and corresponding times in Figs. 8–10. For example, intense boiling occurs within 20 ms for the rougher two surfaces, but is delayed an additional 25 ms for the polished surfaces. The increased vapor production associated with increased roughness leads to a more efficient consumption of liquid and shorter droplet lifetimes in nucleate boiling, as is indeed depicted in the impact regime maps of Fig. 10(a–c).

4. SUMMARY

The present study explored the effects of surface roughness on droplet impact and ensuing heat transfer over broad ranges of Weber number and surface temperature. Key findings from the study are as follows.

(1) Like most boiling systems, heat transfer for impinging droplets can be categorized into the commonly known boiling curve regimes of film, transition and nucleate boiling, in addition to a thin film evaporation regime. However, each of these regimes is characterized by liquid–surface interactions far more complex than those found in other boiling systems. These interactions are influenced to varying degrees by surface roughness.

(2) Surface roughness influences the LFP temperature for impacting droplets quite differently than for sessile droplets. For sessile droplets, surface features penetrate the vapor layer beneath the droplet, yielding higher LFP temperatures for rougher surfaces. For impinging droplets, on the other hand, protruding features on rough surfaces tend to rupture the liquid film resulting from the impact, greatly reducing the pressure beneath the droplet and, therefore, yielding a lower LFP temperature compared to a polished surface.

(3) Impact regime maps have been presented which provide a powerful means of depicting, aside from the commonly known boiling curve regimes, the complex liquid–solid interactions which occur within each regime. The key trends of droplet impact revealed in these maps are (a) a systematic increase of droplet lifetime with decreasing surface temperature, (b) a decreasing droplet spreading time with increasing Weber number, and (c) a more violent breakup of the droplet with increasing Weber number.

(4) Surface features influence the boiling regimes of droplets in two major ways, inducing violent breakup of the spreading liquid film at high temperatures corresponding to film boiling and the upper portion of the transition boiling regime, and increasing nucleation site density at lower temperatures corresponding to nucleate boiling and the lower portion of the transition boiling regime. Enhanced nucleation at the lower temperatures is largely responsible for decreasing droplet lifetime on rougher surfaces.

REFERENCES

1. J. D. Bernardin and I. Mudawar, Validation of the quench factor technique in predicting hardness in heat treatable aluminum alloys, *Int. J. Heat Mass Transfer* **38**, 863–873 (1995).
2. D. D. Hall and I. Mudawar, Experimental and numerical study of quenching complex-shaped metallic alloys with multiple, overlapping sprays, *Int. J. Heat Mass Transfer* **38**, 1201–1216 (1995).
3. D. D. Hall and I. Mudawar, Predicting the impact of quenching on mechanical properties of complex-shaped aluminum alloy parts, *ASME J Heat Transfer* **117**, 479–488 (1995).
4. K. A. Estes and I. Mudawar, Correlation of Sauter mean diameter and critical heat flux for spray cooling of small surfaces, *Int. J. Heat Mass Transfer* **38**, 2985–2996 (1995).
5. I. Mudawar and W. S. Valentine, Determination of the local quench curve for spray-cooled metallic surfaces, *J. Heat Treating* **7**, 107–121 (1989).
6. W. P. Klinzing, J. C. Rozzi and I. Mudawar, Film and transition boiling correlations for quenching of hot surfaces with water sprays, *J. Heat Treating* **9**, 91–103 (1992).
7. J. C. Rozzi, W. P. Klinzing and I. Mudawar, Effects of spray configuration on the uniformity of cooling rate and hardness in the quenching of aluminum parts with nonuniform shapes, *J. Mater. Engng Perform.* **1**, 49–60 (1992).

8. T. M. Anderson and I. Mudawar, Microelectronic cooling by enhanced pool boiling of a dielectric fluorocarbon liquid, *ASME J. Heat Transfer* **111,** 752–759 (1989).
9. J. D. Bernardin and I. Mudawar, An experimental investigation into the relationship between temperature–time history and surface roughness in the spray quenching of aluminum parts, *ASME J. Mater. Technol.* **118,** 127–134 (1996).
10. S. Chandra and S. D. Aziz, The evaporation of a liquid nitrogen droplet on a solid surface, *AIChE Symp. Ser.* **89,** 36–43 (1993).
11. W. S. Bradfield, Liquid–solid contact in stable film boiling, *I EC Fundam.* **5,** 200–204 (1966).
12. M. Cumo, G. E. Farello and G. Ferrari, Notes on droplet heat transfer, *Chem. Engng Prog. Symp. Ser.* **65,** 175–187 (1969).
13. K. J. Baumeister, R. E. Henry and F. F. Simon, Role of the surface in the measurement of the Leidenfrost temperature. In *Augmentation of Convective Heat and Mass Transfer* (Edited by A. E. Bergles and R. L. Webb), pp. 91–101. ASME, New York (1970).
14. S. Nishio and M. Hirata, Study on the Leidenfrost temperatue (2nd report, behavior of liquid–solid surface contact and Leidenfrost temperature), *Trans. JSME* **44,** 1335–1346 (1977).
15. C. T. Avedisian and J. Koplik, Leidenfrost boiling of methanol droplets on hot porous/ceramic surfaces, *Int. J. Heat Mass Transfer* **30,** 379–393 (1987).
16. O. G. Engel, Waterdrop collisions with solid surfaces, *J. Res. N.B.S.* **54,** 281–298 (1955).
17. E. N. Ganic and W. M. Rohsenow, Dispersed flow heat transfer, *Int. J. Heat Mass Transfer* **20,** 855–866 (1977).
18. J. D. Bernardin and I. Mudawar, Mapping of impact and heat transfer regimes of water drops impinging on a polished surface, *Int. J. Heat Mass Transfer* (in press).
19. N. Hatta, H. Fujimoto, H. Takuda, K. Kinoshita and O. Takahashi, Collision dynamics of a water droplet impinging on a rigid surface above the Leidenfrost temperature, *ISIJ Int.* **35,** 50–55 (1995).
20. C. Corty and A. S. Foust, Surface variables in nucleate boiling, *Chem. Engng Prog. Symp. Ser.* **51,** 1–12 (1955).
21. P. J. Berenson, Experiments on pool-boiling heat transfer, *Int. J. Heat Mass Transfer* **5,** 985–999 (1962).
22. L. S. Tong, *Boiling Heat Transfer and Two-Phase Flow.* Wiley, New York (1965).
23. G. P. Nikolayev, V. V. Bychenkov and V. P. Skripov, Saturated heat transfer to evaporating droplets from a hot wall at different pressures, *Heat Transfer—Soviet Res.* **6,** 128–132 (1974).
24. H. Hiroyasu, H. Kadota and T. Sendra, Droplet evaporation on a hot surface in pressurized and heated ambient gas, *Bull. JSME* **17,** 1081–1087 (1974).
25. G. S. Emmerson, The effects of pressure and surface material on the Leidenfrost point of discrete drops of water, *Int. J. Heat Mass Transfer* **18,** 381–386 (1975).
26. S. C. Yao and K. Y. Cai, The dynamics and Leidenfrost temperature of drops impacting on a hot surface at small angles, *Expl. Thermal Fluid Sci.* **1,** 363–371 (1988).
27. V. P. Labeish, Thermohydrodynamic study of a drop impact against a heated surface, *Expl Thermal Fluid Sci.* **8,** 181–194 (1994).